LA-UR- 87-3732

Los Alamos National Laboratory is operated by the University of California for the United States Department of Energy under contract W-7405-ENG-36

TITLE TRAC-PF1/MOD1 CALCULATIONS AND DATA COMPARISONS FOR MIST SMALL-BREAK LOSS-OF-COOLANT ACCIDENTS WITH SCALED 10 cm^2 AND 50 cm^2 BREAKS

LA-UR--87-3732

DE88 003175

AUTHOR(S) J. L. Steiner
D. A. Siebe
B. E. Boyack

SUBMITTED TO 15th Water Reactor Safety Information Meeting
October 26-30, 1987
National Bureau of Standards
Gaithersburg, Maryland

DISCLAIMER

MASTER

Los Alamos Los Alamos National Laboratory
Los Alamos, New Mexico 87545

TRAC-PF1/MOD1 CALCULATIONS AND DATA COMPARISONS FOR MIST SMALL-BREAK LOSS-OF-COOLANT ACCIDENTS WITH SCALED 10 cm^2 AND 50 cm^2 BREAKS*

by

J. L. Steiner, D. A. Siebe, and B. E. Boyack

Safety Code Development Group
Nuclear Technology and Engineering Division
Los Alamos National Laboratory
Los Alamos, New Mexico 87545

ABSTRACT

Los Alamos National Laboratory is a participant in the Integral System Test (IST) program initiated in June 1983 for the purpose of providing integral system test data on specific issues/phenomena relevant to post-small-break loss-of-coolant accidents (SBLOCAs), loss of feedwater and other transients in Babcock & Wilcox (B&W) plant designs. The Multi-Loop Integral System Test (MIST) facility is the largest single component in the IST program. MIST is a 2×4 (2 hot legs and steam generators, 4 cold legs and reactor-coolant pumps) representation of lowered-loop reactor systems of the B&W design. It is a full-height, full-pressure facility with 1/817 power and volume scaling. Two other experimental facilities are included in the IST program: test loops at the University of Maryland, College Park and at Stanford Research Institute. The objective of the IST tests is to generate high-quality experimental data to be used for assessing thermal-hydraulic safety computer codes. Efforts are underway at Los Alamos to assess TRAC-PF1/MOD1 against data from each of the IST facilities.

Calculations and data comparisons for TRAC-PF1/MOD1 assessment have been completed for two transients run in the MIST facility. These are the MIST nominal test, Test 3109AA, a scaled 10 cm^2 SBLOCA and Test 320201, a scaled 50 cm^2 SBLOCA. Only MIST assessment results are presented in this paper.

INTRODUCTION

Los Alamos is currently providing analytical support to the Integral System Test (IST) program; the largest part of our analytical efforts involve the use of the TRAC-PF1/MOD1 code. There are three applications where TRAC is, or has been, used as a complement to the Multi-Loop Integral System Test (MIST) experimental program. The first application is related to test specification or design. During fiscal year 1986, Los Alamos performed five MIST pretest analyses. The experiments were chosen on the basis of their potential either to approach the facility limits or to challenge the predictive capability of the TRAC-PF1/MOD1 code. Three small-break loss-of-coolant accident (SBLOCA) tests were examined that included nominal test conditions, throttled auxiliary feedwater (AFW) and asymmetric steam-generator (SG) cooldown, and reduced high-pressure-injection (HPI) capacity, respectively. Also analyzed were two "feed-and-bleed" cooling tests with reduced HPI and delayed HPI initiation. Results of the tests showed that the MIST facility limits would not be approached in the five tests considered. The second application is related to test evaluation. It is impossible to include all the desired instrumentation in a facility. Constraints of cost, complexity, space, etc., are rapidly reached. If one has sufficient confidence that TRAC will correctly predict the dominant test phenomena, calculations can be used to fill in gaps about quantities that are not measured in the facility. The third application is related to TRAC assessment. The ability of a thermal-hydraulic code to accurately calculate experimental behavior in scaled facilities is an important link in demonstrating that the code can be used to predict how an operating pressurized water reactor would perform under accident conditions. During fiscal year 1987, Los Alamos performed two MIST posttest analyses. The two experiments were chosen on the basis of their potential to challenge the predictive capability of the TRAC code. These tests are identified and briefly discussed in the following paragraphs.

* This work was funded by the US Nuclear Regulatory Commission, Office of Nuclear Regulatory Research, Division of Accident Evaluation.

Test 3109AA MIST test 3109AA was the nominal test for the MIST program. During the early test program several repeats of the specified nominal test were run. The test selected for the nominal Test 3109AA differs from the pretest specification for 310000 in the initial pressurizer liquid level and efforts to warm the surge line and maintain the pressurizer liquid at saturation until test initiation. The nominal conditions include a scaled 10-cm^2 cold-leg (CL) discharge leak, full HPI and AFW, reactor-coolant pumps (RCPs) not available, no noncondensible gas injection, automatic reactor vessel vent valve (RVVV) actuation on differential pressure, automatic guard heater control, constant steam generator (SG) secondary level control after SG refill, and symmetric SG cooldown.

Test 320201 This test differed from the nominal in that the scaled leak size was increased from 10 cm^2 to 50 cm^2. Other specified conditions and procedures for the test were the same.

Most experiments scheduled for the first year of operation of the MIST facility have been completed. Tests 3109AA and 320201 are from test groups 31 and 32 for which formal test reports have been submitted to IST program participants for review. Data tapes for the posttest analyses of tests 3109AA and 320201 were obtained in a preliminary form prior to the completion of final data qualification by Babcock & Wilcox (B&W).

CODE VERSIONS

We used updated versions of the TRAC-PF1/MOD1 code (Ref. 1). The TRAC-PF1/MOD1 code was developed at Los Alamos National Laboratory to provide advanced best-estimate predictions of postulated accidents in light-water reactors. The code features a two-phase, two-fluid nonequilibrium hydrodynamics model with a noncondensible gas field, flow-regime-dependent constitutive equation treatment; either one- or three-dimensional treatment of the reactor vessel; complete control-systems modeling capability, a turbine component model, and a generalized steam-generator component model.

Code versions 12.7 and 14.3 were used for the analysis of tests 3109AA and 320201 respectively. Code modifications were necessary for this application. Initialization of the MIST facility in natural circulation rather than pumped flow caused modeling difficulties unique to this facility. An accurate prediction of SG heat-transfer distribution is necessary to correctly predict steady-state loop flows and hence initial system pressure and temperatures. Code and model modifications were necessary to achieve this. These are expected to be applicable only to the MIST facility and are used only with the model for it.

PLANT MODEL

Figure 1 is a MIST facility arrangement drawing. Figures 2 and 3 provide an overview of the TRAC MIST facility model. The TRAC model of the MIST facility has evolved over a period of time. The model was initially based on preliminary information provided in the MIST Facility Specification. It has progressed to its present form as available as-built facility information was received from B&W. The model consists of 77 components that have been subdivided into 251 fluid cells. Only one-dimensional components are used in this model. The model is considered to be rather finely noded and is expected to predict the dominant phenomena during MIST experiment.

CALCULATION RESULTS

During analysis of our calculations, we found that many of the predicted phenomena occurred in each of the calculations. Therefore, we have chosen to provide a detailed description of nominal MIST Test 3109AA and a less detailed description for the posttest prediction for Test 320201. The discussion in this case focuses on the important phenomena that differ from those in the nominal case. We note that for each test calculation, at time zero, the primary was liquid full and coolant was being driven by natural circulation.

TEST 3109AA CALCULATION

The TRAC-PF1/MOD1 posttest calculation for Test 3109AA was performed for the first 7000 s of the experiment. During this time period, all of the major phenomena took place and the automatic safety systems and emergency operating procedures were activated. At the end of the 7000 s calculational period, the HPI flow exceeded the leak flow and refilling of the primary system was well underway.

Steady-State Calculation

The TRAC-PF1/MOD1 steady-state calculation for Test 3109AA was performed for 2000 s corresponding to approximately five loop transients. At the end of the steady-state calculation the primary- and secondary-system fluid conditions had stabilized within the uncertainties of the measured values.

Transient Calculation

The observed and calculated thermal hydraulic phenomena and system interactions are discussed in detail in this section. The discussion is divided into four transient phases; these phases are defined with reference to Fig. 4, the primary and secondary pressure response. Data is denoted by a dashed line and calculated values by a solid line.

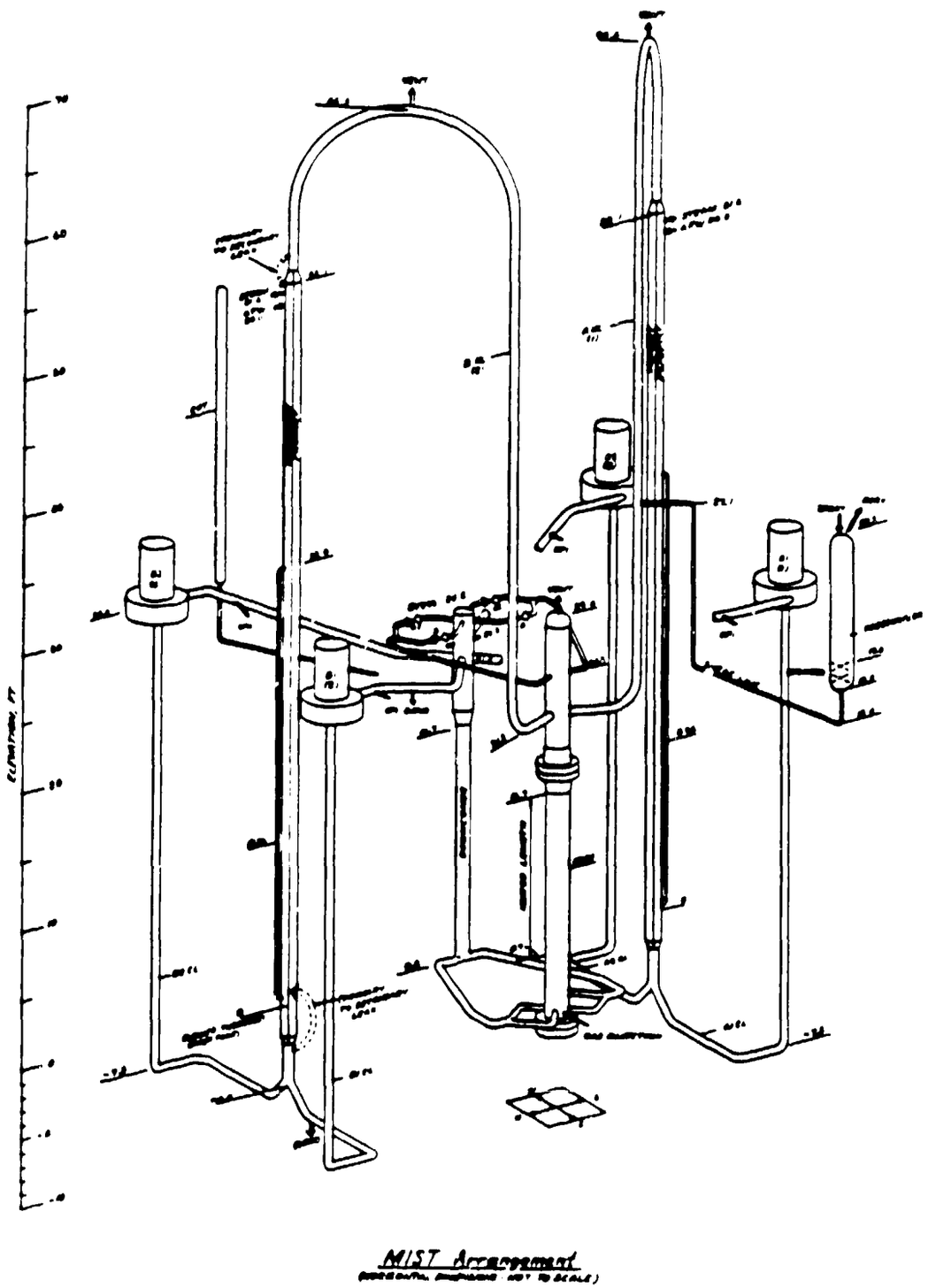

Fig. 1.
MIST facility isometric

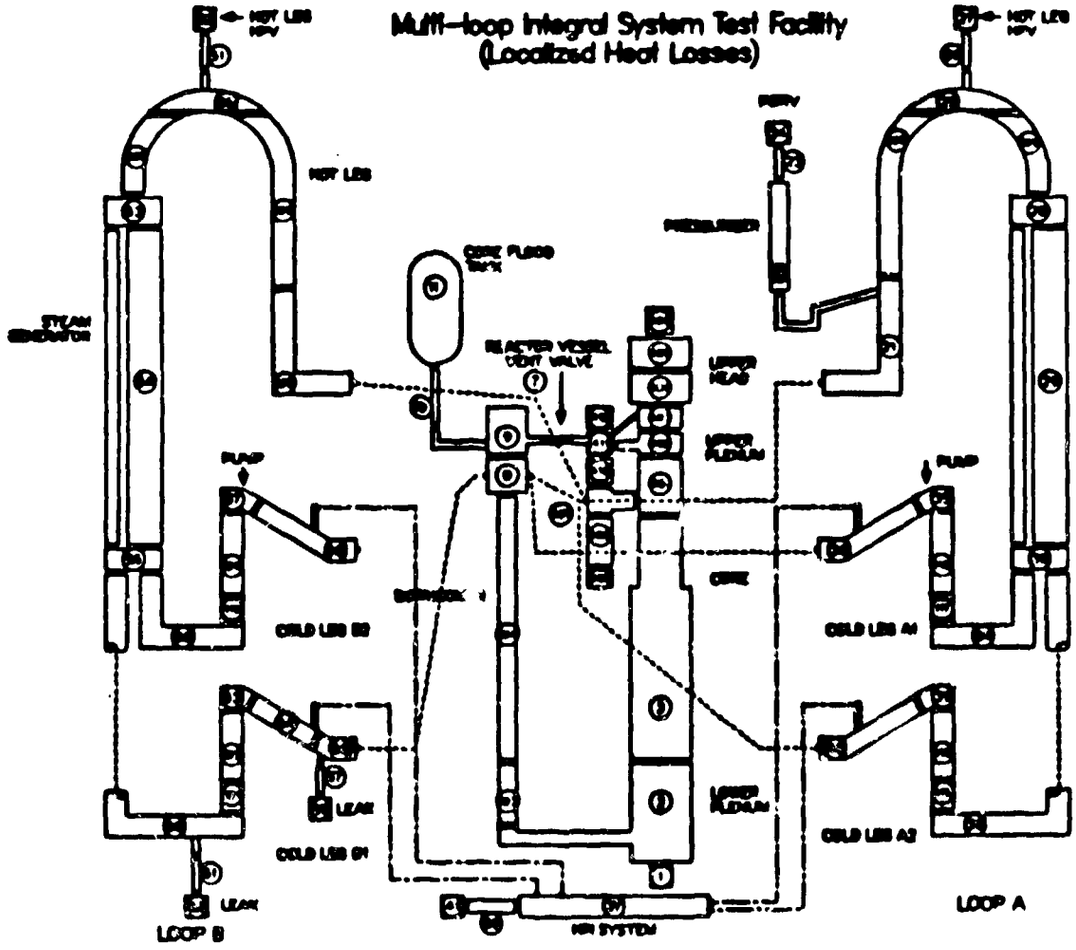

Fig. 2.
TRAC component noding schematic of MIST facility

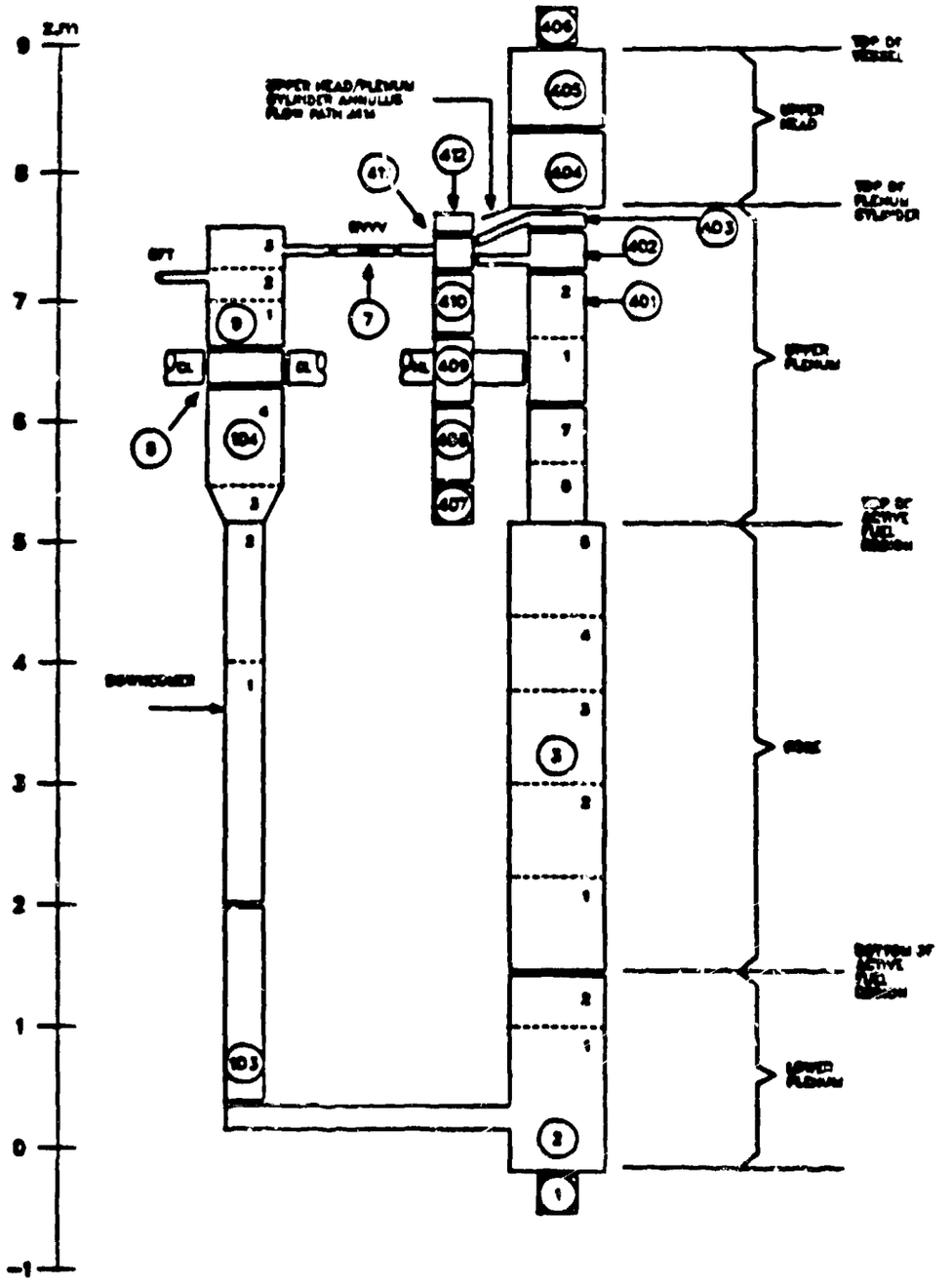

Fig. 3.
TRAC reactor-vessel noding schematic of MIST facility

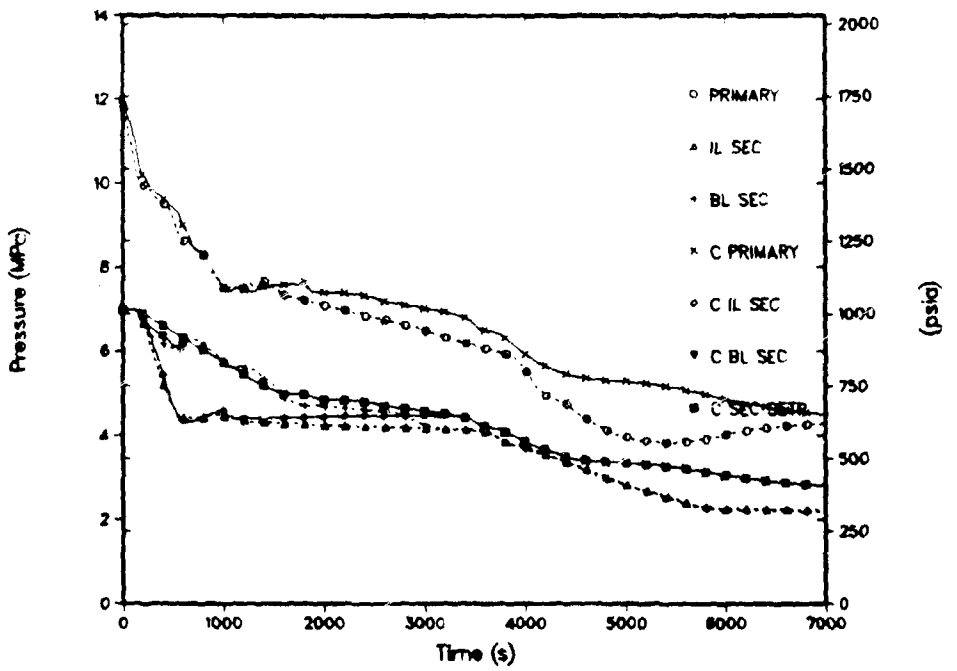

Fig. 4.
Test 3109AA primary and secondary pressures.

A "C" as the first letter in the curve label denotes a calculated value. Phase one, subcooled decompression, covers the period from the start of the transient to 185 s when the intact-loop hot leg saturates and the depressurization rate is reduced. Phase two, intermittent circulation, covers the period of continued depressurization, repressurization, and termination of repressurization from 185 s to 1870 s when natural circulation is terminated in the loops. Phase three, loop stagnation, covers the period of gradual depressurization from 1875 s to approximately 4000 s when primary-system refill begins. Phase four, refill, extends from the beginning of refill at 4000 s to the end of the calculation at 7000 s. A summary of the major events for Test 3109AA is presented in Table I.

TABLE I

EVENT TABLE FOR TEST 3109AA

Test Time (s)	Calculation Time (s)	Event Description
0.0	0.0	Start transient—break initiation
150.0	160.0	Pressurizer level drops to 0.3048 m (1.0 ft), core power ramp, HPI, RVVV automatic control initiated, RVVV first opens, SG secondary level reset
185.0	185.0	Intac-loop hot leg saturates
240.0	31[illegible]0	Intact-loop flow ends
1575.0	1840.0	Intermittent broken-loop flow ends
4000.0	3430.0	Beginning of refill
	7000.0	Calculation terminated

Phase One, Subcooled Decompression Phase one is the first part of the transient from leak initiation until the saturation pressure was reached in the hot legs at 185 s. During phase one, the fluid in the primary system was subcooled liquid and the primary-system pressure decreased rapidly as the liquid expanded due to the leak flow. At the end of phase one, the primary-system depressurization rate was reduced by flashing of the liquid in the hot legs.

At the beginning of the transient, the primary system was in steady-state single-phase natural circulation. The driving force for natural circulation was the density difference between the hot fluid in the hot legs and vessel and colder fluid in the SG tubes, CLs, and downcomer. The test was initiated at time zero by opening a scaled 10-cm^2 leak in the B1 CL just downstream of the HPI port. This caused an immediate reduction in the calculated primary-system pressure (Fig. 4) and pressurizer level as a result of the flow of liquid through the leak. The liquid initially in the pressurizer was near saturation temperature, and as this liquid was discharged into the intact-loop hot leg, it mixed with the hot-leg fluid resulting in a higher fluid temperature in the intact-loop hot leg relative to the broken-loop hot leg. Since the density of the liquid in the intact-loop hot leg was thereby reduced, the intact-loop natural-circulation flow increased at the beginning of the transient as shown in Fig. 5.

The level in the pressurizer drained down to the 0.3048 m (1-ft) level at 150 s in the test and at 160 s in the calculation. At these times the following control actions were taken: core power decay was started, HPI flow was started, the RVVVs were transferred to automatic control, the AFW level control set point was changed from 1.52 m (5 ft) to 9.63 m (31.6 ft), and the abnormal transient operator guidelines (ATOG)-based pressure-control logic was initiated for the SG secondaries. This automated SG secondary pressure control was used to archive modelable and reproducable boundary conditions while approximating plant ATOG control. The pressurizer low-level trip was reached 10 s earlier in the test because of the higher measured leak flow at the beginning of the transient (Fig. 6).

The effect of the core power decay after the pressurizer low-level trip was to increase the measured and calculated primary depressurization rates as shown in Fig. 4. The depressurization rate was high at this time because all of the primary fluid was still subcooled and expanding because of the leak flow. Also at the time of the low-level trip, the RVVVs were switched from manually closed to automatic control based on differential pressure. Figures 7 and 8 show that the vent valves opened immediately, causing a brief reduction in both loop flows at 150 s in the calculation and 160 s in the test. The reduction in the loop flows was then followed by a recovery in both loops (Figs. 5 and 9) with the sharpest recovery in the intact loop. This increase in the loop flows was a result of the increased AFW flow (Figs. 10 and 11) in response to the AFW set-point change at 150 s in the calculation and 160 s in the test. The loop flows were increased by the AFW flow because the AFW raised the thermal center in the SG; the intact-loop flow was increased more since the pressurizer was still discharging hot fluid into the intact loop at this time.

Figure 5 shows that the increase in the intact-loop flow was abruptly terminated at approximately 185 s in both the calculation and the experiment. At this time the primary-system pressure (Fig. 4) had decreased to the saturation pressure of the intact-loop hot-leg fluid. Flashing of the hot-leg fluid then created a vapor bubble in the intact-loop hot-leg U-bend (Fig. 12) and the natural-circulation flow in the intact loop was interrupted as shown in Fig. 5. The intact-loop saturation marked the end of phase one at 185 s. Subsequent depressurization of the primary system was then inhibited by flashing of the fluid in the intact-loop hot leg, as shown in Fig. 4, which indicates a reduction in the measured and calculated primary-system depressurization rates at 185 s.

Differences between the calculation and the experiment during phase one resulted primarily from the higher measured leak flow (Fig. 6). This caused a slightly higher depressurization rate (Fig. 4) and an earlier occurrence of the pressurizer low-level trip in the test.

Phase Two, Intermittent Circulation. Phase two covers the period of intermittent circulation in the loops after the first saturation of loop fluid occurs in the intact-loop hot leg. During phase two, the natural circulation flow in each loop was governed by the liquid level in the hot leg in that loop. As the hot leg liquid level receded, the U-bend was uncovered and the loop flow was quickly terminated. Also during phase two, the SG AFW and steam flows responded to the control procedures started during phase one when the pressurizer level decreased to 0.3048 m (1 ft). At the beginning of phase two the AFW was on in both SGs as the levels were being raised to the 9.36 m (31.6 ft) set point, and throughout phase two, the secondary pressures were controlled to a variable set point based on ATOG. The ATOG set point is determined from the core exit temperature and the saturation temperatures corresponding to the SG secondary pressures as described in Ref. 2. Depending on these three temperatures, the set point pressure may be (1) held constant, (2) reduced by $5.746 \cdot 10^{-3}$ MPa/s (50 psi/min), or (3) reduced such that the corresponding saturation temperature is reduced by 55.56 K/h (100°F/h). The logic for determining which of these pressure-control modes is to be used is explained in detail in Ref. 2. Phase two extends to 1575 s in the test and 1870 s in the calculation, when the flow in the broken loop is terminated by the uncovery of the broken-loop hot-leg U-bend.

After the saturation of the intact-loop hot leg fluid at the end of phase one, the liquid level in the intact-loop hot leg decreased rapidly (Fig. 12) as a result of continued flashing. Figure 5 shows that as a result, the intact-loop

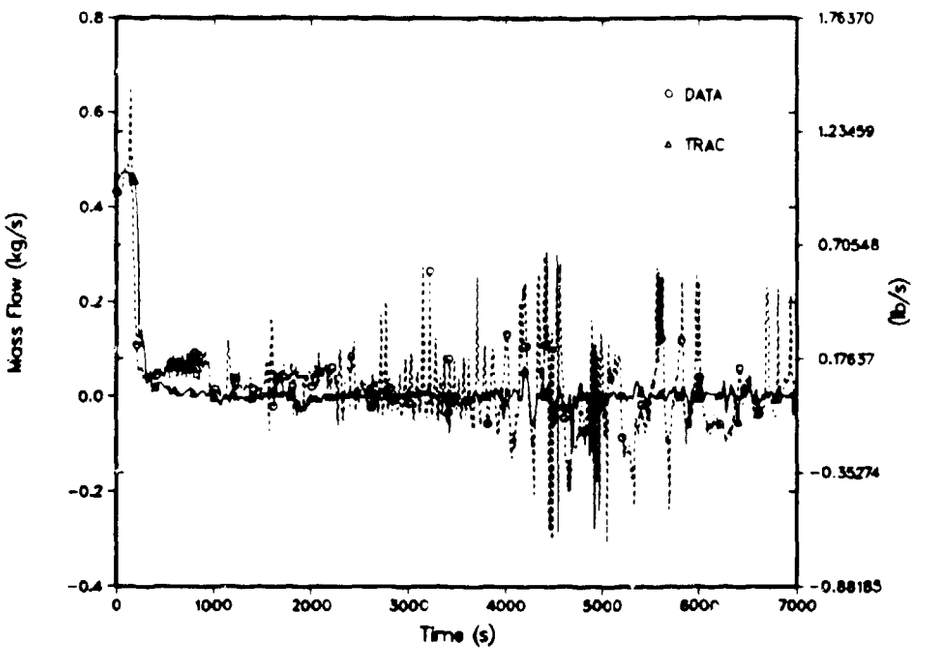

Fig. 5.
Test 3109AA total intact-loop CL flow.

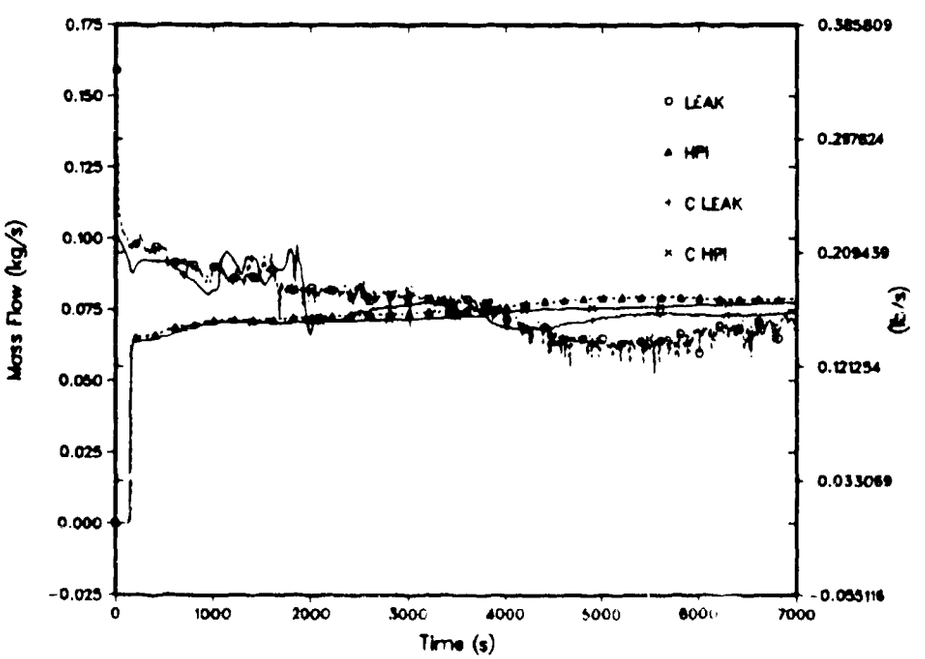

Fig. 6.
Test 3109AA CL leak and HPI flows.

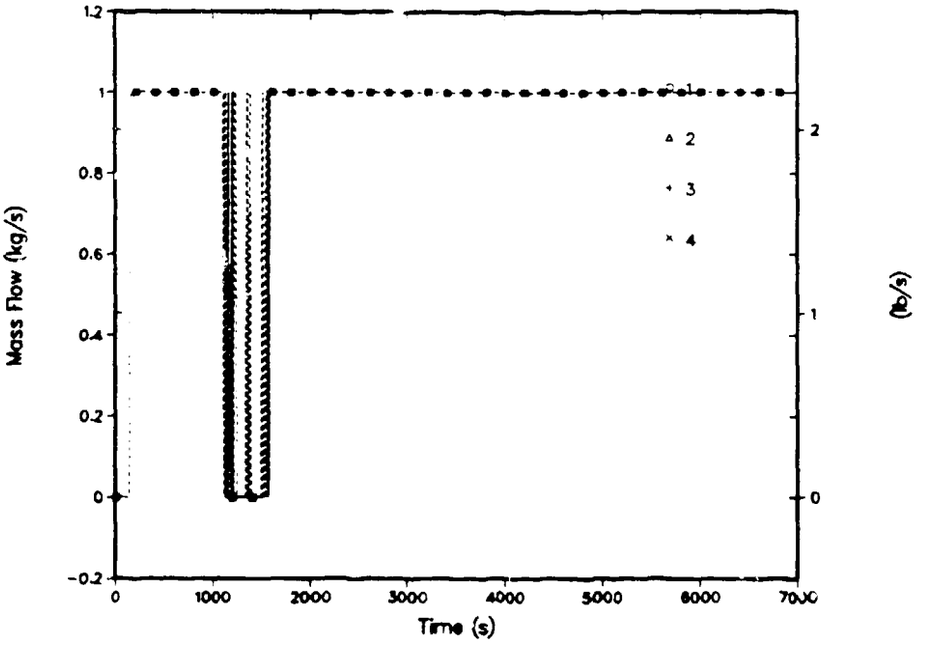

Fig. 7.
Test 3109AA MIST vent valve full closed indicator (test).

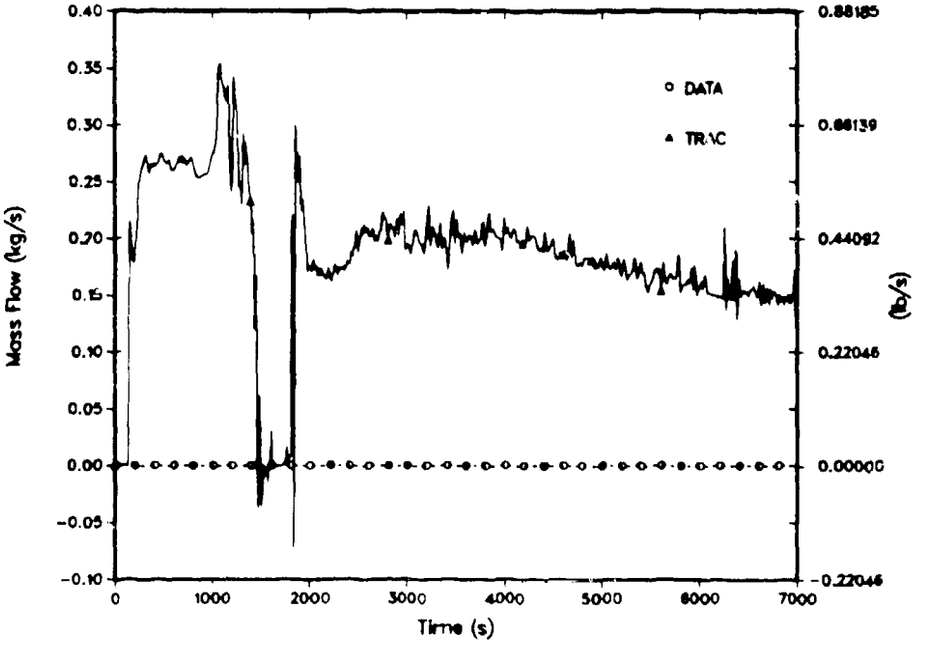

Fig. 8.
Test 3109AA RVVV flows

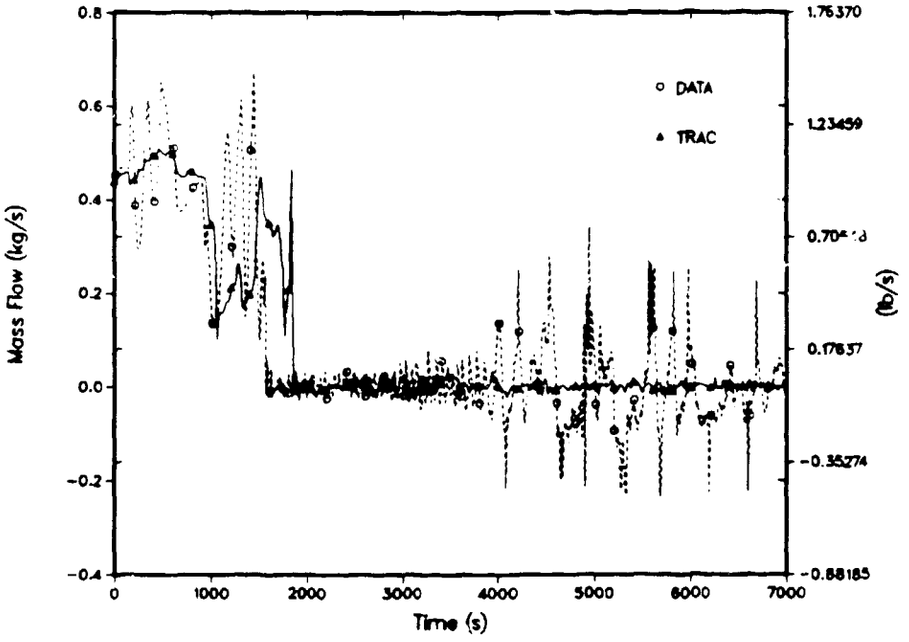

Fig. 9.
Test 3109AA total broken-loop CL flow.

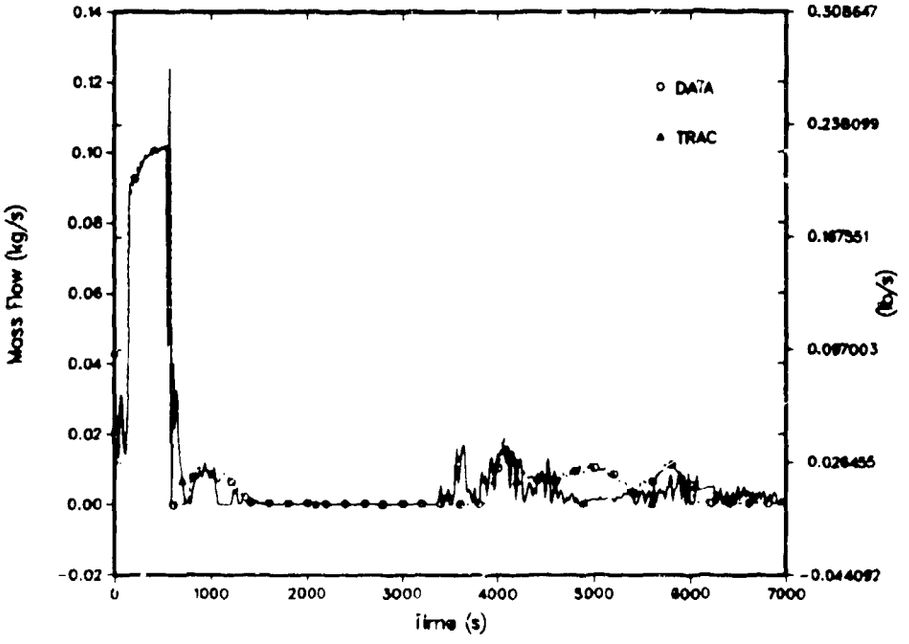

Fig. 10.
Test 3109AA intact loop SG AFW flow.

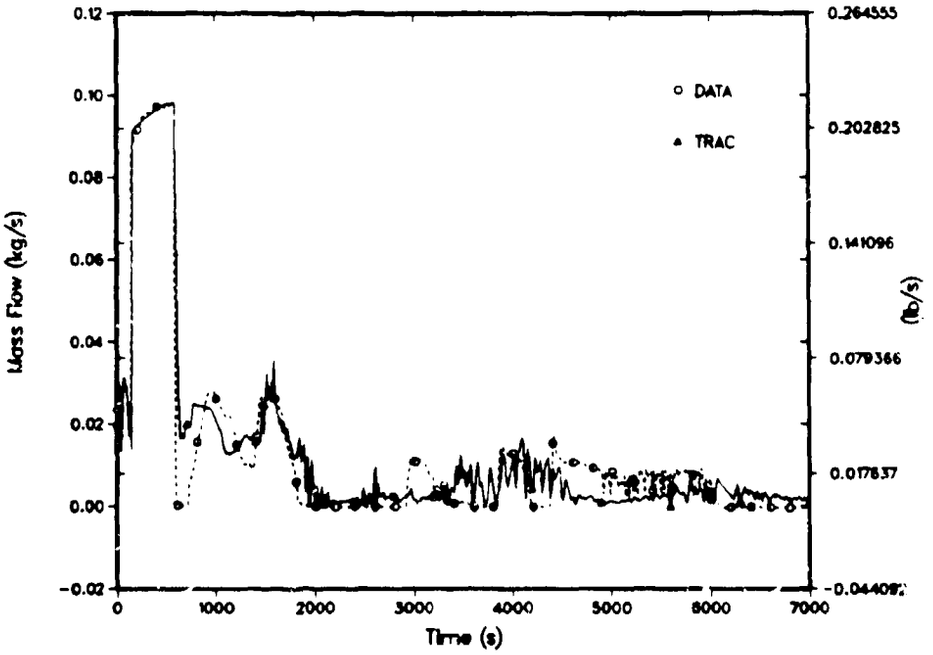

Fig. 11.
Test 3109AA broken-loop SG AFW flow

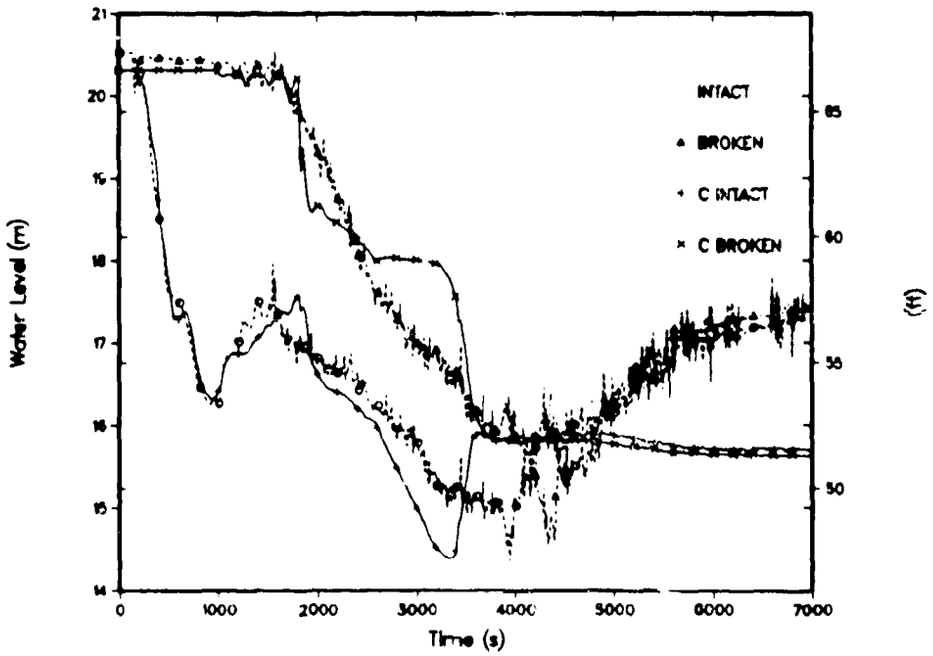

Fig. 12.
Test 3109AA hot-leg collapsed liquid levels

natural-circulation flow was terminated by 240 s in the test and 310 s in the calculation and was not reestablished. Heat transfer in the intact-loop SG then ceased because of the loss of natural circulation in the intact loop. In the absence of heat transfer from the primary, the intact-loop SG secondary pressure decreased from the ATOG set point in both the test (at 240 s) and in the calculation (at 310 s) as shown in Fig. 4. This decrease, caused by the AFW flow into the intact-loop SG (Fig. 10), continued until the level (Fig. 13) reached the 9.63 m (31.6 ft) set point at 565 s in both the test and the calculation and the AFW flow decreased (Fig. 10). After the intact-loop SG secondary pressure fell below the ATOG set point, the steam flow in the intact-loop secondary was terminated (Fig. 14) by the pressure controller.

When the intact-loop SG secondary was refilled to the 9.63-m (31.6-ft) level in the experiment, the AFW controller was switched into a constant-level control mode and a proportional-integral controller was used to maintain the SG level at the 9.63-m (31.6-ft) set point. This control mode change affected the AFW flow after the intact loop SG was refilled at 565 s. Figure 10 shows that after 565 s, the AFW flow was briefly terminated and then restarted from 800 to 1500 s while the SG level settled in on the 31.6 ft set point. When the AFW was restarted in the intact-loop SG, vapor was present in the primary side of the tubes at the 15.48 m (50.8 ft) AFW elevation (Fig. 13) and condensation heat transfer began immediately. This boiler condenser mode (BCM) heat transfer began in both the test and the calculation at 565 s resulting in a more rapid primary depressurization (Fig. 4). The BCM was terminated at 1000 s in both the test and the calculation when the intact-loop SG primary level (Fig. 13) increased to the AFW elevation and condensation in the primary was terminated.

Without steam flow, AFW flow was not required to maintain the level in the intact-loop SG after the 31.6 ft set point was achieved and Fig. 10 shows that the AFW flow was completely terminated in the intact loop after 1500 s in both the test and the calculation. The intact-loop SG therefore remained inactive after 1500 s while its pressure was below the ATOG set point.

The system interactions in the broken loop during phase two were similar to those just described in the intact loop. However, the timing of events in the broken loop was delayed because the broken loop hot leg fluid was cooler than the fluid in the intact-loop hot leg at the beginning of phase two. Figure 12 shows that the broken-loop hot leg was maintained liquid full until 1000 s as the intact-loop hot-leg level receded as a result of local flashing. Beginning at approximately 850 s, however, the intact-loop level fell at a slower rate as it approached the liquid level in the primary side of the intact-loop SG (Fig. 12). With the slower draining in the intact-loop hot leg, the broken-loop hot leg level eventually began to recede at 1000 s as indicated in Fig. 12. The natural-circulation flow in the broken loop (Fig. 9) then began to decrease rapidly at approximately 1000 s, in both the test and the calculation, in response to the decrease in the broken-loop hot-leg level. This reduction of flow in the broken loop had two effects. First, the heat transfer in the broken-loop SG started to decrease, leading to an increase in the primary-system pressure and corresponding decrease in broken-loop secondary pressure beginning at 1000 s (Fig. 4). Second, the core-outlet flow was diverted into the upper head and through the RVVVs as shown in Fig. 8. The repressurization of the primary system retarded the flashing in both the intact and broken loops and, at the same time, flashing increased in the upper head due to the diverted core outlet flow. As a consequence, both the measured and calculated intact-loop hot-leg levels started to increase at 1000 s while the vessel level decreased more rapidly, as shown in Figs. 12 and 15.

The final sequence of events in phase two started at 1000 s with the intact-loop hot-leg levels increasing and the vessel levels decreasing as described above. The increased rate of upper head voiding in both the test and the calculation at 1000 s was sufficient to terminate the reduction in the broken-loop natural-circulation flow (Fig. 9), which then began to increase. As flashing continued in the upper head, the vessel level receded, as shown in Fig. 15, and at 1250 s in the test (1385 s in the calculation) the RVVV nozzles were uncovered. As a result, the RVVV flow began to decrease rapidly at this time and was completely terminated at 1150 s in the test and at 1480 s in the calculation as shown in Figs. 7 and 8. The broken-loop spillover flows (Fig. 9) were sharply increased by the RVVV closures at these times in both the test and the calculation. Shortly afterward, however, the broken-loop U-bend uncovered (Fig. 12) as the primary system continued to drain and the natural-circulation flow in the broken loop started to decrease rapidly, as shown in Fig. 9. The broken-loop natural-circulation flow then continued to decrease and was completely interrupted at 1575 s in the test and at 1870 s in the calculation. During this final decrease in broken-loop natural-circulation flow, Figs. 7 and 8 show that the RVVVs reopened at 1575 s in the test and at 1840 s in the calculation when the downcomer drained to the RVVV elevation (Fig. 16) and remained open thereafter.

During the period when the RVVVs were closed, Fig. 9 shows a strong natural-circulation flow in the broken loop. The effect of this flow was to increase the heat transfer in the broken loop SG and also to mix cold HPI fluid with hotter fluid in the primary system. As a result, the primary system repressurization which began at 1000 s was terminated at 1575 s in the test and 1875 s in the calculation.

The termination of spillover circulation in the broken loop at 1575 s in the test and 1870 s in the calculation marks the end of phase two. Major events during phase two occurred slightly earlier in the test than in the calculation

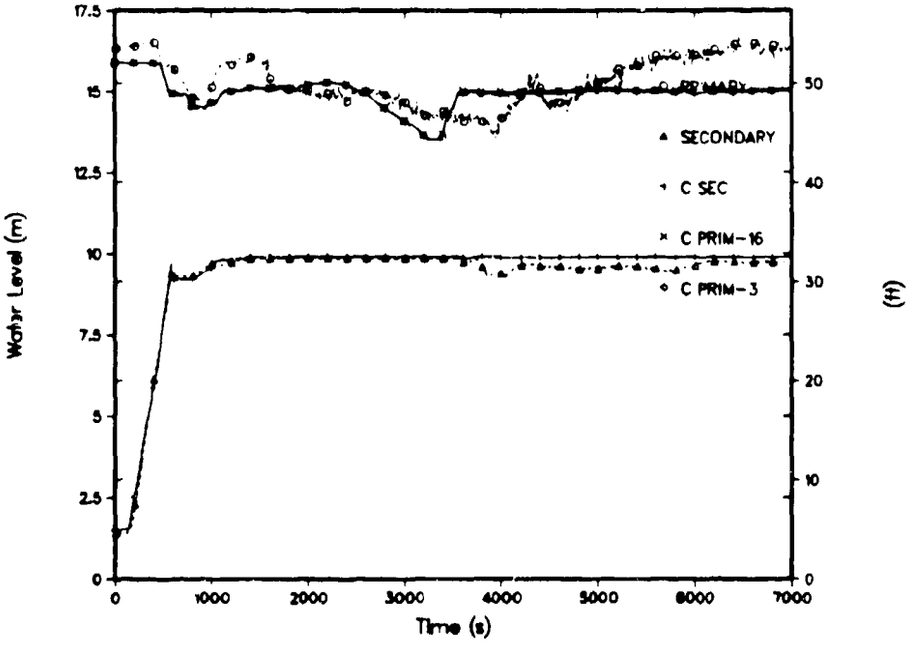

Fig. 13.
Test 3109AA intact-loop SG collapsed liquid levels

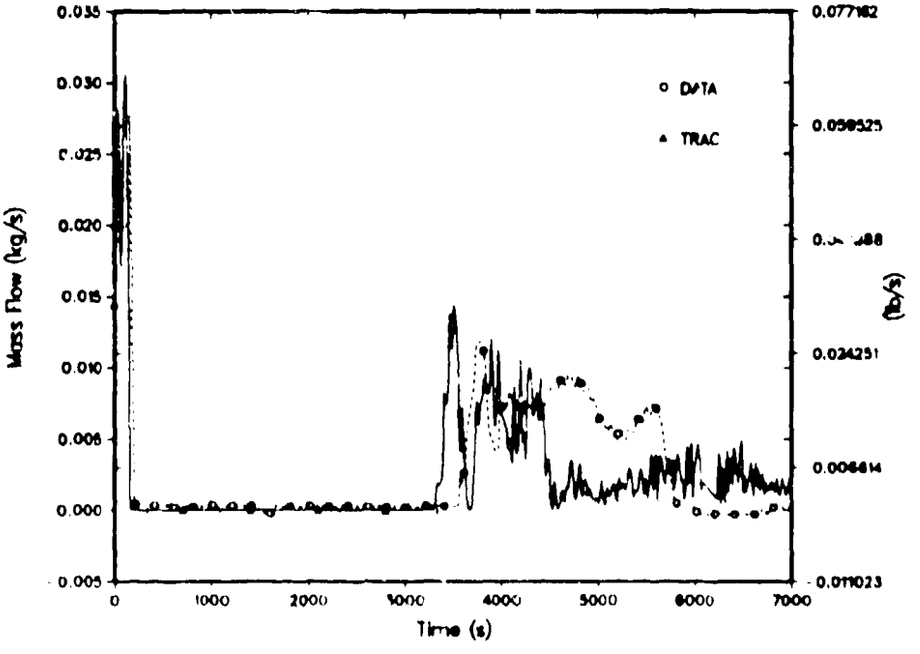

Fig. 14.
Test 3109AA intact loop SG secondary steam flow

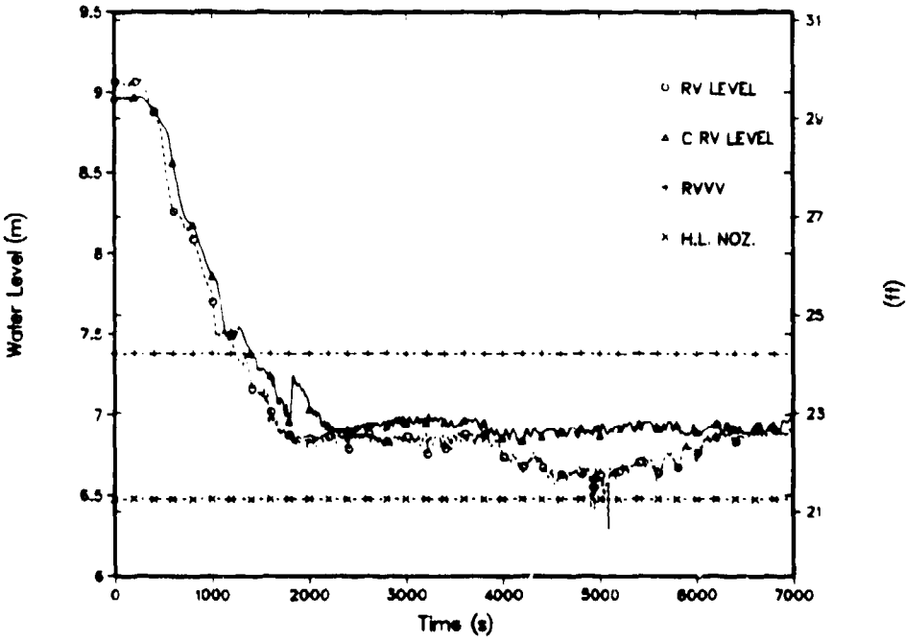

Fig. 15.
Test 3109AA reactor vessel collapsed liquid level

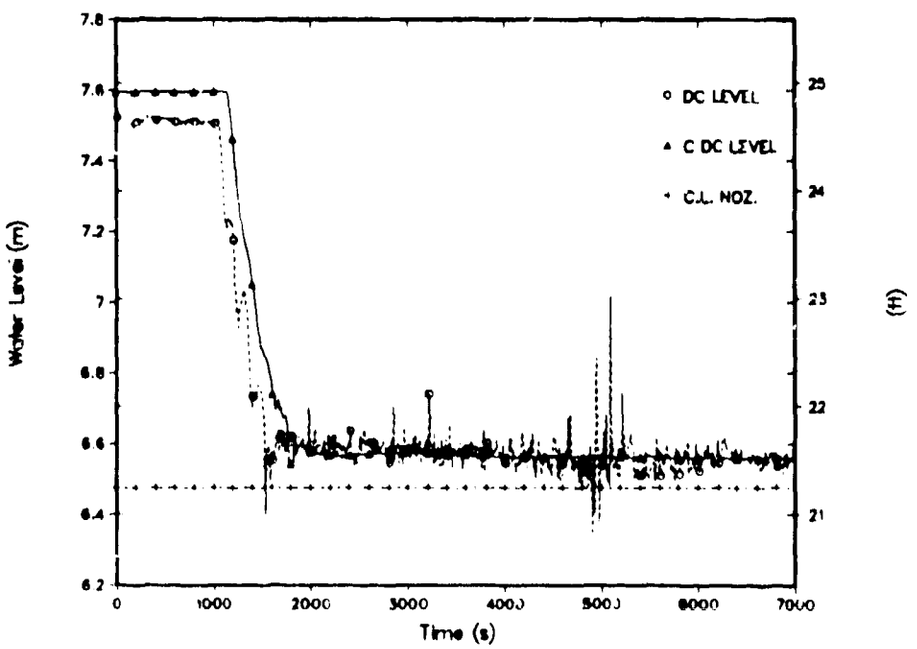

Fig. 16.
Test 3109AA downcomer collapsed liquid level

because of the higher leak flow in the test from test initiation to 1080 s. At the end of phase two, in both the test and the calculation, the primary system was depressurizing, the broken-loop SG secondary pressure was being controlled to the decreasing ATOG set point, and AFW was controlling the SG level in the broken loop. The intact-loop SG was inactive at the end of phase two since its pressure was below the ATOG set point.

Phase Three, Loop Stagnation. Phase three is the period of stagnated natural-circulation flow in the loops after the final spillover in the broken loop. During phase three the primary system was cooled by the leak/HPI feed and bleed and by AFW in the broken loop SG. The primary-system pressure decreased during phase three as a result of core power decay and the leak/HPI cooling. Phase three ended at 4000 s in the test and 3400 s in the calculation when AFW was restarted in the intact loop and the primary-system depressurization rate was increased.

During most of phase three, the primary was cooled by the leak/HPI feed and bleed and by AFW in the broken loop (Fig. 11). Most of the cooling was done by the feed and bleed; at 3000 s, for example, Fig. 6 shows that in the test, the HPI flow was approximately 0.074 kg/s (0.1628 lb/s) and the leak upstream temperature (Fig. 17) was 524.9 K. The energy required to heat this HPI flow to the temperature at the leaksite, 72 kW, was greater than the 59 kW core power at this time. In the calculation at 3000 s, the HPI flow was slightly lower (0.0716 kg/s), 71 kW was needed to heat this flow to the leak upstream temperature in the calculation, and the core power was also 59 kW at 3000 s. The primary-system pressure decreased during phase three as a result of the decreasing core power and excess energy removal of the leak/HPI cooling.

At the beginning of phase three, a circulation flow developed in the broken-loop CLs in both the test and the calculation. The CL circulation flow began immediately after the broken-loop U-bend spillover flow was terminated at the end of phase two. At this time, fluid from the downcomer was drawn toward the leak site and the flow in the B1 CL reversed. The CL circulation flow was then maintained by the density difference between the B1 and B2 CLs resulting from the flow of warmer fluid from the downcomer into the B1 CL. The circulation flow was important because it affected the leak upstream temperature (Fig. 17) in both the test and the calculation.

Figure 17 shows that the broken loop CL circulation flow caused a reduction of approximately 30 K in the fluid subcooling upstream of the leak in the test as well as in the calculation. The corresponding reduction in the leak flow (Fig. 6) at 1930 s in the calculation, however, was larger than the reduction observed in the test at 1660 s. This difference apparently indicates that the TRAC-PF1/MOD1 critical flow model did not properly account for the change in leak upstream subcooling in the calculation. After the initial decrease in leak flow at the beginning of phase three, Figs. 6 and 17 show that the calculated leak flow gradually recovered toward the measured value as the subcooling increased in the calculation.

The lower calculated leak flow during phase three resulted in a lower depressurization rate in the calculation (Fig. 4) and slower loop draining (Fig. 12). Figure 12 shows that after the broken loop interrupted in the test, the broken-loop hot-leg level remained above the intact-loop level, and both loops drained at approximately the same rate. The difference in hot-leg levels resulted from a temperature difference between the intact and broken loop the hot leg piping. After the flow in each U-bend voided and the loop flow interrupted, the U-bend piping temperature was maintained by the guard heaters at approximately the saturation temperature at the time of the interruption. Since the intact loop interrupted earlier when the saturation temperature was higher, the intact-loop U-bend piping temperature stayed higher after both loops had interrupted. The higher piping temperature created a higher vapor pressure in the intact-loop U-bend relative to the broken-loop U-bend; and because of this pressure difference, the intact-loop hot-leg level remained below the broken-loop hot-leg level during phase three.

The same draining behavior, with the higher level in the broken-loop hot leg, occurred in the calculation during phase three. However, after 2600 s in the calculation, the draining in the broken loop was halted and the leak was then fed by accelerated draining of the intact loop (Fig. 12). This transition at 2600 s in the calculation is currently under further study. It appears that a change occurred in the calculation at this time which affected the heat transfer from the piping to the vapor in one of the U-bends. The difference in the observed and calculated hot-leg draining rates after 2600 s, however, did not cause other calculated parameters to diverge from the measured values. Figures 4, 6, and 17 show no change in the calculated leak upstream temperature, leak flow, or primary-system pressure at 2600 s.

During phase three, the primary and secondary conditions were such that the ATOG set-point pressure was approximately equal to the saturation pressure corresponding to a temperature 27.78 k (50°F) below the core exit temperature. This is evidenced in Fig. 4, which shows that during phase three, the calculated ATOG pressure decreased at the same rate as the primary pressure. The difference in the corresponding saturation temperatures during this decrease was approximately 27.78 K (50°F). Fig. 4 shows that the difference between the primary and ATOG pressures was nearly constant during phase three in the test and in the calculation.

The SG secondary pressure control is important because it affects the AFW flow in each SG. The AFW flow depends on the pressure control because AFW is used to control the secondary levels. If the secondary pressure is being reduced then AFW will be required to maintain the secondary level. During phase three, the broken loop AFW

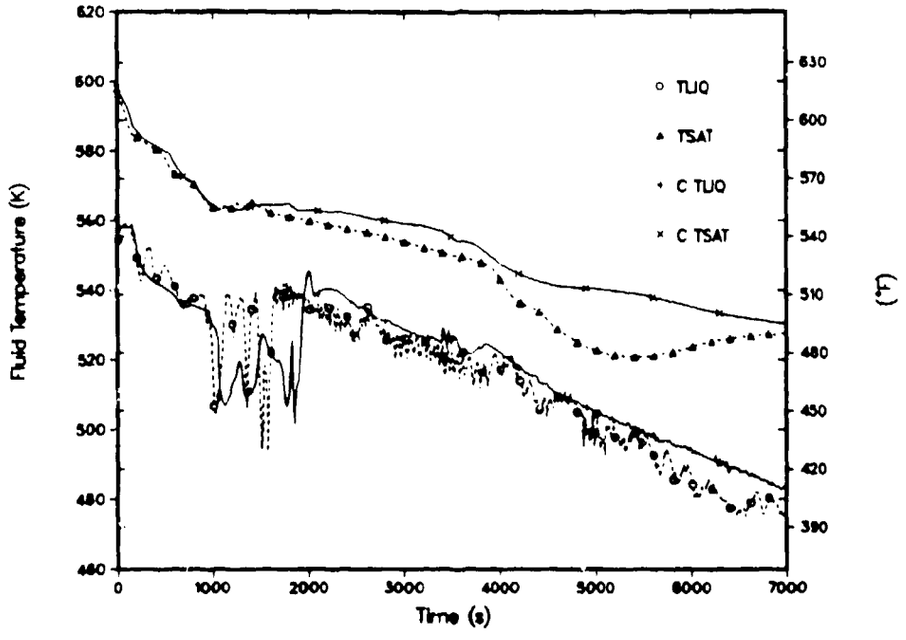

Fig. 17.
Test 3109AA leak upstream fluid temperatures.

was on (Fig. 11) in both the test and the calculation because the broken loop SG secondary pressure was controlled to the decreasing ATOG set point (Fig. 4). The intact-loop AFW was off (Fig. 10), however, since the intact-loop SG secondary pressure was below the ATOG set point (Fig. 4), and therefore the intact-loop steam flow was controlled to zero (Fig. 14).

Figure 4 shows that in the test, the intact-loop SG pressure remained constant during phase three when the AFW and steam flows were off. The calculated intact-loop SG pressure, however, increased slightly during phase three. This may have occurred because the steam-line heat losses modeled (1.5 kW per steam line) were too low. The test may have also had other losses, such as leakage of steam through the control valve, that contributed to the stability of the secondary pressures that were not modeled. The increase in the intact-loop SG pressure during phase three caused the decreasing ATOG set-point pressure to be reached at 3400 s in the calculation (4000 s in the test) as shown in Fig. 4. At these respective times, AFW was restarted in the intact loop leading to BCM which marked the end of phase three in both the test and the calculation.

Phase Four, Refill. Phase four covers the period from the beginning of the BCM in the intact loop until the end of the calculation at 7000 s. During phase four, the primary-system pressure was reduced by AFW boiler condenser mode heat transfer in the intact-loop SG causing the HPI flow to exceed the leak flow. The calculation was terminated at 7000 s, since at this time it was evident that the point of minimum primary system inventory had been reached.

At the end of phase three, the ATOG set-point pressure decreased to the intact-loop SG secondary pressure (Fig. 4), causing the steam and AFW flows to be restarted in the intact-loop at 4000 s in the test and at 3400 s in the calculation. This caused extensive condensation heat transfer in the primary side of the intact-loop SG tubes since the level in the tubes was well below the 15.48 m (50.8 ft) AFW-injection elevation (Fig. 13) at this time. As a result, the primary to secondary heat transfer in the intact loop SG was increased at these times and the primary system began to depressurize rapidly in the test and the calculation (Fig. 4).

When the AFW was restarted in the intact loop, the pressure of the vapor inside the SG tubes was reduced by condensation. The liquid level in the intact loop SG and hot leg then rose rapidly while the levels in the broken loop fell. This occurred in both the test and in the calculation, as shown in Fig. 12. However, the level in the broken loop

SG (Fig. 18) fell below the 15.48 m (50.8-ft) AFW elevation in the test but not in the calculation. Therefore the intact-loop BCM in the test was immediately followed by a BCM in the broken loop and the overall reduction in the primary pressure (Fig. 4) was greater in the test than in the calculation.

The effect of the primary-system depressurization at 4000 s in the test and 3400 s in the calculation was to increase the HPI flow above the leak flow as shown in Fig. 6. This event marks the beginning of the refill period. After the start of refill, the levels in the intact and broken loops started to increase as shown in Figs. 13 and 18. The refill rate (excess of HPI flow over leak flow) was higher in the test because of the larger BCM depressurization in the test (Fig. 4). The higher refill rate in the test resulted in correspondingly higher primary-system level increases after refill began in the test as shown in Figs. 6 and 4. The primary system continued to depressurize rapidly in the test (Fig. 4) until the SG primaries were filled above the upper tube sheets (Figs. 13 and 18) and the condensation heat transfer was terminated at approximately 5200 s. This event still had not been reached by the end of the calculation at 7000 s because of the lower refill rate in the calculation.

The differences between the test and the calculation discussed above involved three separate phenomena. First, the critical flow model in TRAC apparently did not properly account for the changes in the leak upstream temperature. Consequently, the calculated leak flow and primary depressurization rates were too low during phase three. Second, the TRAC input model did not include enough heat or steam losses for the secondary side. This allowed the intact-loop SG to pressurize slightly during phase three in the calculation and thereby reach the ATOG set point too soon. Phase three was therefore terminated 600 s early in the calculation. Third, the magnitude of the BCM heat transfer was apparently too low at the beginning of phase four in the calculation. Even though the condensation surface area and AFW flow during this BCM in the calculation matched the data, the primary-system depressurization during the BCM was too low in the calculation. This then caused a lower refill rate during phase four in the calculation.

The overall comparison of the TRAC-PF1/MOD1 calculation for Test 3019AA with measured data from the test was reasonable; this means that the major trends were predicted correctly in the calculation, although TRAC values were frequently outside the range of data uncertainty because of minor code/model deficiencies. With reasonable agreement, correct conclusions will still be reached when the code is used in similar applications.

TEST 320201 CALCULATION

The TRAC-PF1/MOD1 posttest calculation for Test 320201 was performed for the first 2800 s of the experiment. During this period, all of the major events occurred and the automatic safety systems and emergency operating procedures were activated. At the end of the 2800 s calculational period, the HPI and accumulator flows exceeded the leak flow and refilling of the primary system was well underway.

Steady-State Calculation

The TRAC-PF1/MOD1 steady-state calculation for Test 320201 was also performed for 2000 s (approximately 5 loop transits). At the end of the steady-state calculation, the primary and secondary system fluid conditions had stabilized within the uncertainties of the measured values.

Transient Calculation

The comparison of the observed and calculated thermal hydraulic phenomena and system interactions is discussed in this section. Test 320201 was exactly like Test 3109AA except that a (scaled) 50-cm^2 leak orifice was used instead of a 10-cm^2 orifice. The purpose of the test was to investigate the effects of increased leak size on the SBLOCA behavior. Many of the same phenomena occurred during Test 320201 as occurred in Test 3109AA; however, the magnitude of the phenomena and the timing of major events were altered by the larger leak size. In the following discussion, the phenomena are explained in less detail than for Test 3109AA and the emphasis is placed on the analysis of the differences between the calculation and the test. The analysis is somewhat limited, however, by the fact that measured mass flow rates in the loops and downcomer are not available for this test. The discussion of this SBLOCA transient is again divided into four phases; these phases are defined with reference to Fig. 19, the primary and secondary pressure response. Phase one, subcooled decompression, covers the period from the start of the transient to approximately 20 s when the loop hot-leg fluid saturated and the depressurization rate was reduced. Phase two, spillover circulation, covers the period of continued depressurization and brief pressure stabilization from 20 s to 100 s when natural circulation was terminated in the loops. Phase three, loop stagnation, covers the period of depressurization from 100 s to approximately 1760 s in the test (1650 s in the calculation) when primary system refill began. Phase four, refill, then extends to the end of the calculation at 2800 s. A summary of the major events for Test 3109AA is presented in Table II.

Phase One, Subcooled Decompression. Phase one is the first part of the transient from leak initiation until the saturation pressure was reached in the hot legs at 20 s. During phase one, the fluid in the primary system was subcooled liquid, and the primary system pressure decreased rapidly as the liquid expanded as a result of the leak

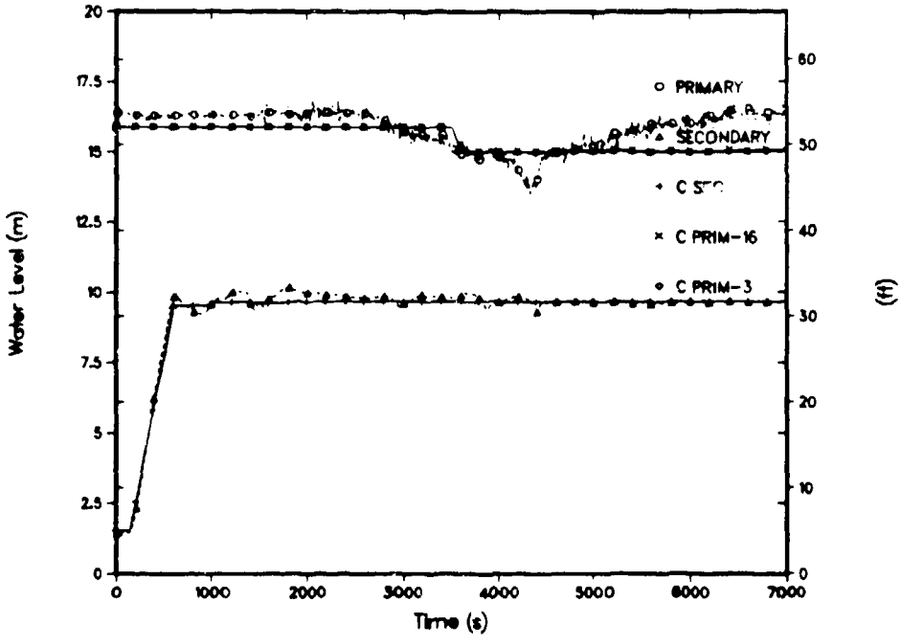

Fig. 18.
Test 3109AA broken looop SG collapsed liquid levels.

TABLE II
EVENT TABLE FOR TEST 20201

Test Time (s)	Calculation Time (s)	Event Description
0.0	0.0	Start transient break initiation.
20.0	20.0	Hot legs saturate
40.0	38.0	Pressurizer level drops to 0.3048 m (1.0 ft), core power ramp, HPI RVVV automatic control initiated, RVVV first opens, SG secondary level reset
100.0	100.0	Loop flows terminate
1760.0	1650.0	Beginning of refill
	2800.0	Calculation terminated

flow. At the end of phase one, the primary-system depressurization rate was reduced by flashing of the liquid in the hot legs.

At the beginning of the transient, the primary system was in steady state single phase natural circulation and the test was initiated at time zero by opening a scaled 50 cm^2 leak in the B1 CL just downstream of the HPI injection port. This caused a sharp reduction in the primary-system pressure (Fig. 19) and a rapid increase in the leak flow (Fig. 20). The leak flow in the experiment exceeded the capacity of the leak flow meter for the first 170 s (Ref. 3). Fig. 20 indicates a constant measured value of 0.43 kg/s during this period. Figure 21, however, shows good agreement between the measured and calculated primary system mass inventories during phase one.

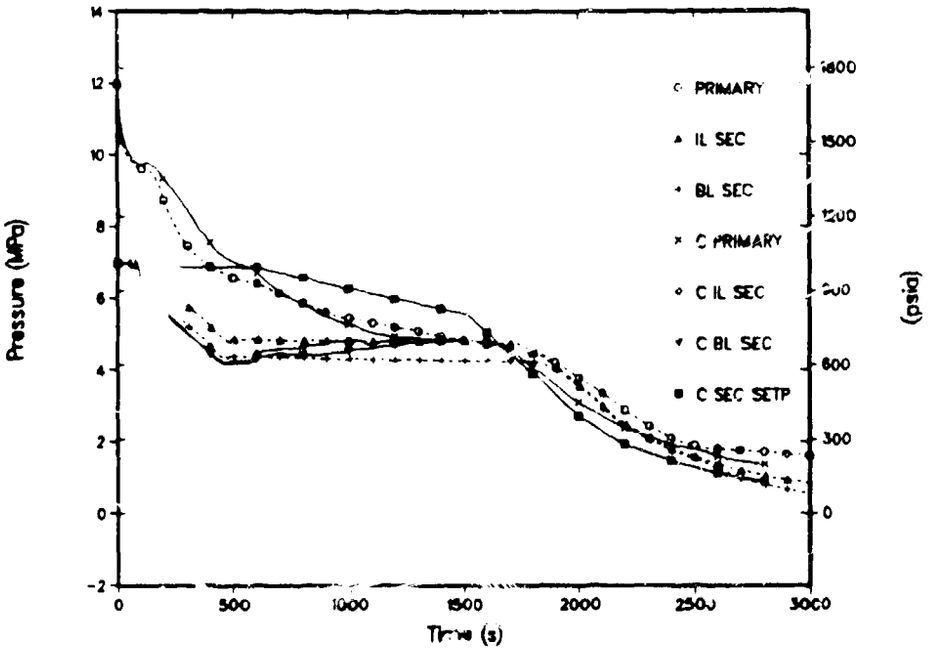

Fig. 19.
Test 320201 primary and secondary pressures.

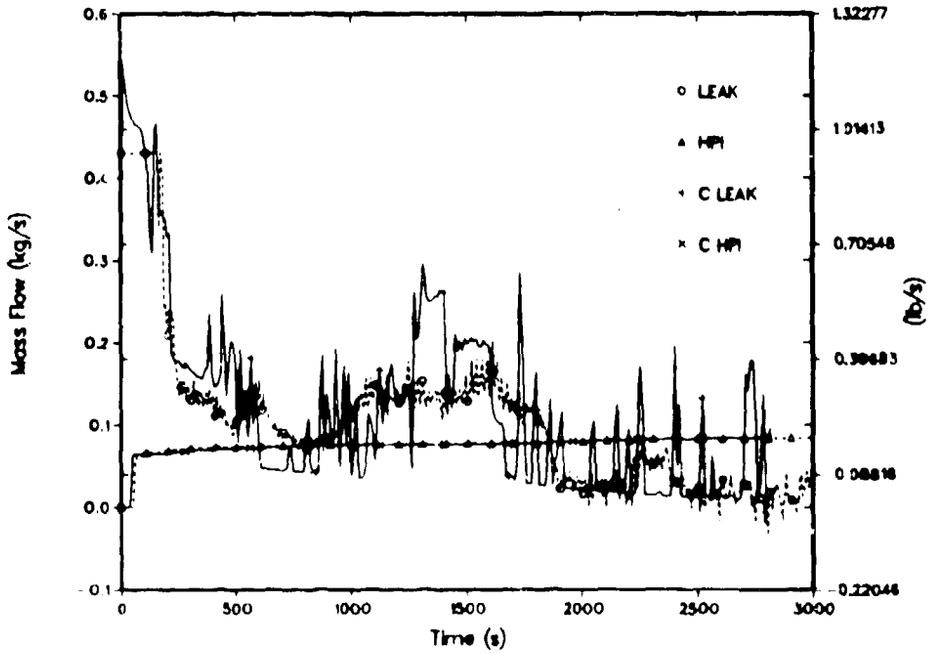

Fig. 20.
Test 320201 CL leak and HPI flows

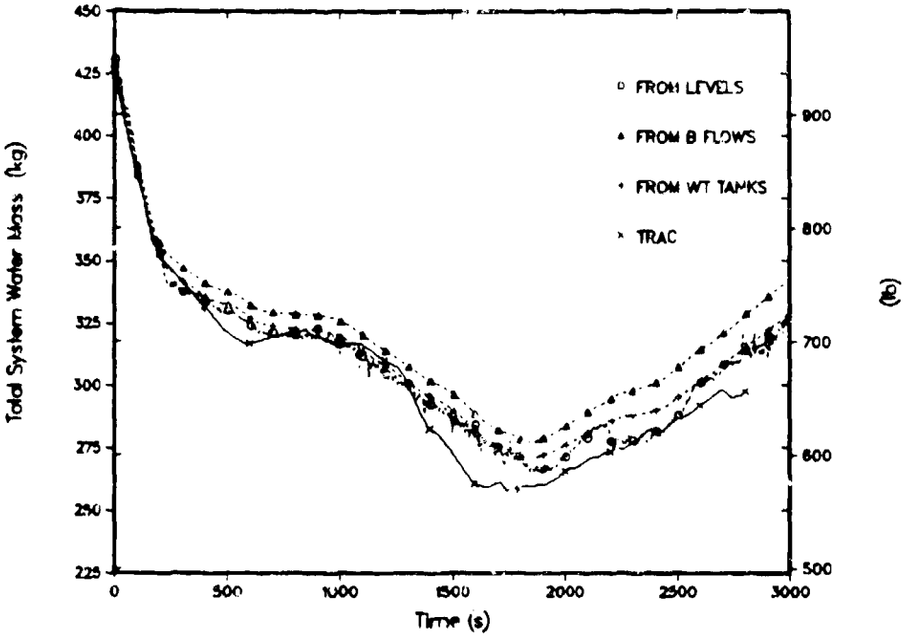

Fig. 21.
Test 320201 primary system water mass

Phase one was terminated at approximately 20 s in both the test and in the calculation when the saturation pressure was reached in the hot legs. Figure 19 shows that the primary-system depressurization rate was reduced at this time as a result of flashing in the hot legs. Because of the increased leak size in Test 320201, phase one ended before the 0.3048 m (1 ft) pressurizer low-level trip had occurred in either the test or the calculation.

Phase Two, Spillover Circulation. Phase two covers the brief period of spillover circulation in the loops after the first saturation of loop fluid occurred in the hot legs. During phase two, the natural-circulation flow in each loop quickly coasted down as the hot-leg levels receded from the U-bends. Also during phase two, the pressurizer level decreased to 0.3048 m (1 ft) and the control procedures for the core power, SG level and pressure control, and RVVVs were reset as described previously. Phase two extends to 100 s, when the flow in each loop was completely terminated by the uncovery of the hot-leg U-bends.

After the saturation of the intact-loop hot-leg fluid at the end of phase one, the liquid level in the intact-loop hot legs decreased (Fig. 22) because of continued flashing and the loop flows began to subside. In the calculation, the U-bend flows (Fig. 23) were approximately the same during phase two and both decreased to zero at 100 s. This same behavior apparently took place in the test, although the measured flows are not available. The AFW was started at 40 s in the test (38 s in the calculation) on pressurizer low-level trip. Figure 19 shows that after 40 s in the test, the SG pressures both fell at the same rate due to the AFW flow. The symmetric secondary response to the AFW flow in the test during phase two indicates that the loop flows were also symmetric in the test. Therefore, it is concluded that the spillover flows in the test were in good agreement with the calculated spillover flows.

When the loop flows were interrupted at the end of phase three at 100 s, SG heat transfer was lost and Fig. 19 shows that the primary-system pressure briefly stabilized in both the test and the calculation. The agreement between the measured and calculated primary pressures during phase two is further evidence that the spillover loop flows were calculated correctly.

Phase Three, Loop Stagnation. Phase three is the period of stagnated natural-circulation flow in the loops after the final spillover in the U-bends. During phase three, the primary was depressurized by BCM heat transfer which began in both loops during the SG refill. Also during phase three, heat transfer in the broken loop SG affected the draining rate of liquid through the primary side of the broken loop SG. This draining then influenced the leak site

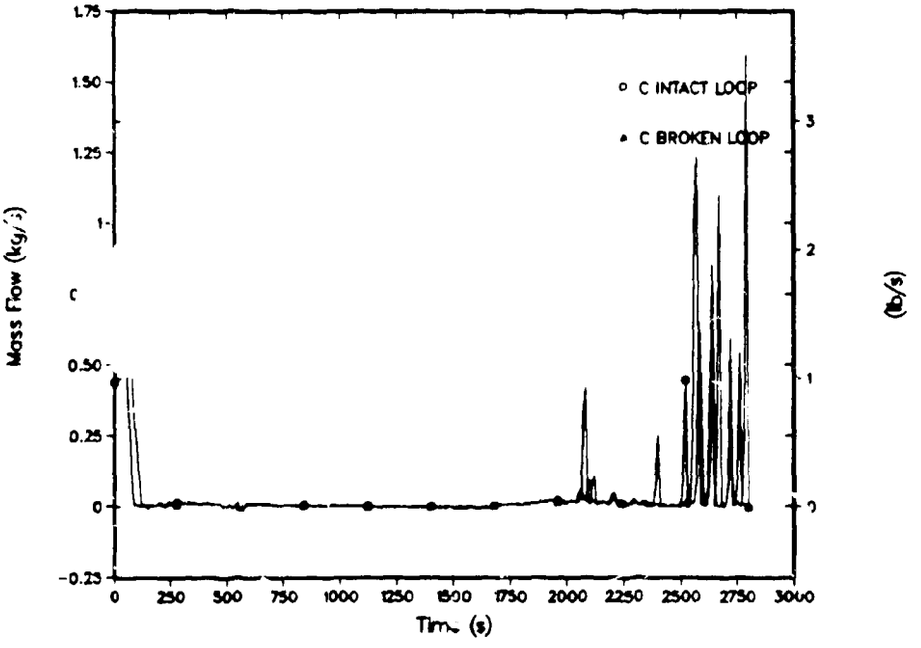

Fig. 22.
Test 320201 hot leg collapsed liquid levels

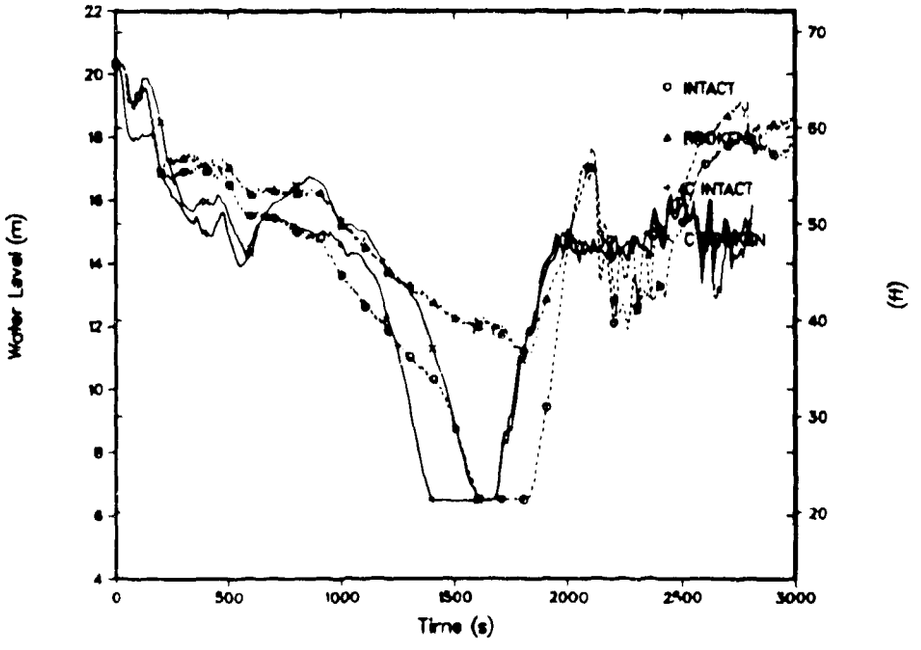

Fig. 23.
Test 320201 calculated hot leg U bend mass flows

which began in both loops during the SG refill. Also during phase three, heat transfer in the broken-loop SG affected the draining rate of liquid through the primary side of the broken loop SG. This draining then influenced the leak site fluid conditions and the leak flow rate. Phase three ended at 1760 s in the test and 1650 s in the calculation when AFW was restarted in the intact loop and the primary-system depressurization rate was increased.

At the beginning of phase three, the SG refill which was started on the low-level pressurizer trip in phase two was still in progress. Figures 24 and 25 show that in both the test and the calculation the SG primary levels fell below the 15.48 m (50.8 ft) AFW elevation before the secondaries were refilled. This occurred at approximately 170 s in the intact loop and 190 s in the broken loop. At these times condensation (BCM) began in the SG primaries. The BCM heat transfer was relatively large because of the high AFW flows during the SG refill. Fig. 19 shows that the primary system depressurized rapidly in both the test and the calculation.

The magnitude of the BCM heat transfer in the calculation was apparently too low in the intact loop. Figure 19 shows that after BCM started in the intact loop at 170 s, the calculated secondary pressure in the intact loop continued to decrease whereas the measured value briefly increased. Figure 19 also shows that the primary depressurization rate at this time was too low in the calculation, further evidence of insufficient primary-to-secondary heat transfer. At the same time, Fig. 24 shows that the calculated primary-side level was below the measured level in the intact-loop SG indicating that the condensing surface area at the inner tube surfaces was greater in the calculation. This indicates that the BCM heat transfer in the intact loop was underpredicted because the effects of the BCM were less pronounced in the calculation while the condensation surface area available was greater in the calculation.

The BCM during phase three was briefly interrupted at the end of SG refill when the AFW in each loop was terminated to transfer the AFW controllers to the constant-level-control mode as described previously. The duration of the AFW termination and the subsequent measured AFW flow until the constant SG levels were achieved in the test were used as boundary conditions in the calculation. Figure 19 shows that when the AFW flow was off from 490 to 575 s, the depressurization rate was reduced in both the test and the calculation. When the AFW flow was restarted and the BCM resumed at 575 s, the subsequent depressurization (Fig. 19) was more rapid in the calculation because the SG primary levels (Figs. 24 and 25) were lower in the calculation at this time. These levels were lower in the calculation because the calculated leak flow (Fig. 20) was generally higher than in the test before 575 s and the primary system inventory (Fig. 21) was lower in the calculation.

The AFW termination from 490 s to 575 s affected other system parameters both in the test and in the calculation. Figure 25 shows that when the AFW was off, the liquid receded faster in the broken-loop SG primary because the vapor above was not being cooled by the AFW. The increased liquid flow from the broken-loop SG primary then fed the leak with colder fluid causing an increase in the measured and calculated leak flows (Fig. 20) during this period.

The draining of liquid from the SG primaries was also affected by the primary-to-secondary heat transfer after AFW flow was terminated at approximately 1200 s when the 9.63 m (31.6 ft) level set point was achieved (Figs. 24 and 25). The draining behavior after this time differed between the test and the calculation because of differences between the measured and calculated SG secondary pressures. In the test, the intact-loop SG pressure increased at 170 s during the BCM as described above, and afterward, the intact-loop SG pressure was higher than the broken-loop SG pressure. Consequently, the saturation temperature difference between the primary and SG secondary was higher in the broken loop, and there was more heat transfer from the primary to the broken loop SG during phase three in the test. Since the fluid in the intact-loop SG primary had less heat loss to the secondary, flashing and draining occurred faster in the intact-loop SG primary in the test, and Fig. 24 shows that the intact-loop SG primary drained faster after 1200 s.

In the calculation, the SG secondary pressures (Fig. 19) increased gradually during phase three as a result of the insufficient heat or steam losses in the model secondary discussed earlier. The intact-loop SG secondary pressure increased slightly faster than the broken loop because of small differences in the primary levels and primary-to-secondary heat transfer. After 1200 s in the calculation, both SG primary levels fell rapidly with the intact-loop SG level falling slightly. The SG primary-level decrease was more uniform in the calculation than in the test because the SG secondary pressures were closer to each other in the calculation. In both the test and the calculation, the draining of the SG primaries supplied the leak with cold fluid resulting in increased leak flow after 1200 s (Fig. 20).

Phase three was terminated at 1760 s in the test and at 1650 s in the calculation when the primary pressure decreased to the highest SG secondary pressure and the blowdown mode of secondary pressure control was started. Phase three ended earlier in the calculation because of the gradual secondary pressure increase after AFW was terminated in the calculation, and because the primary-system depressurized more rapidly in the calculation after AFW was restarted at the end of SG refill.

Phase Four, Refill. Phase four covers the period beginning with the SG secondary blowdown until the end of the calculation at 2800 s. BCM heat transfer was reestablished in both SGs at the beginning of phase four, and

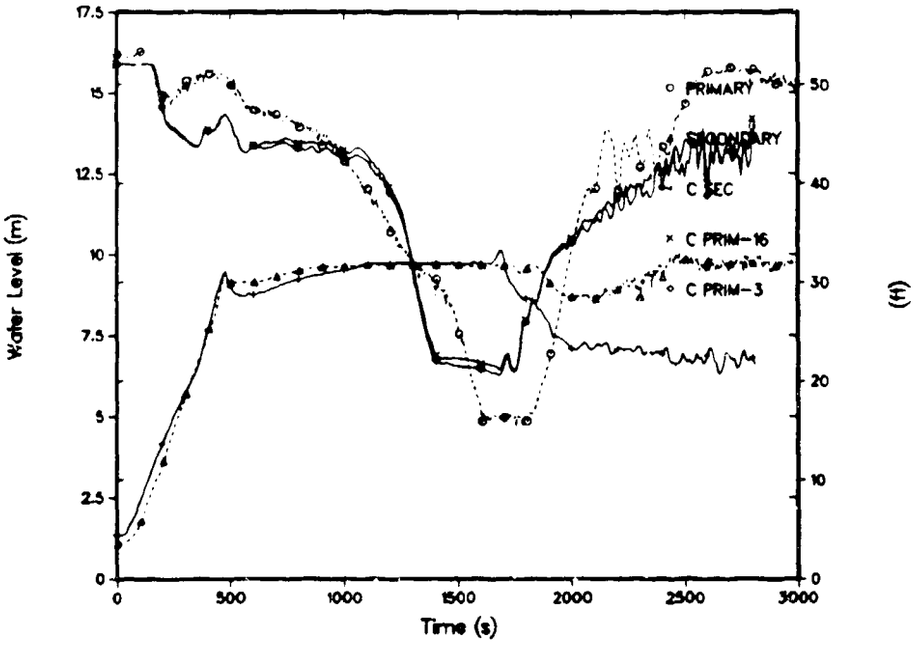

Fig. 24.
Test 320201 intact loop SG collapsed liquid levels.

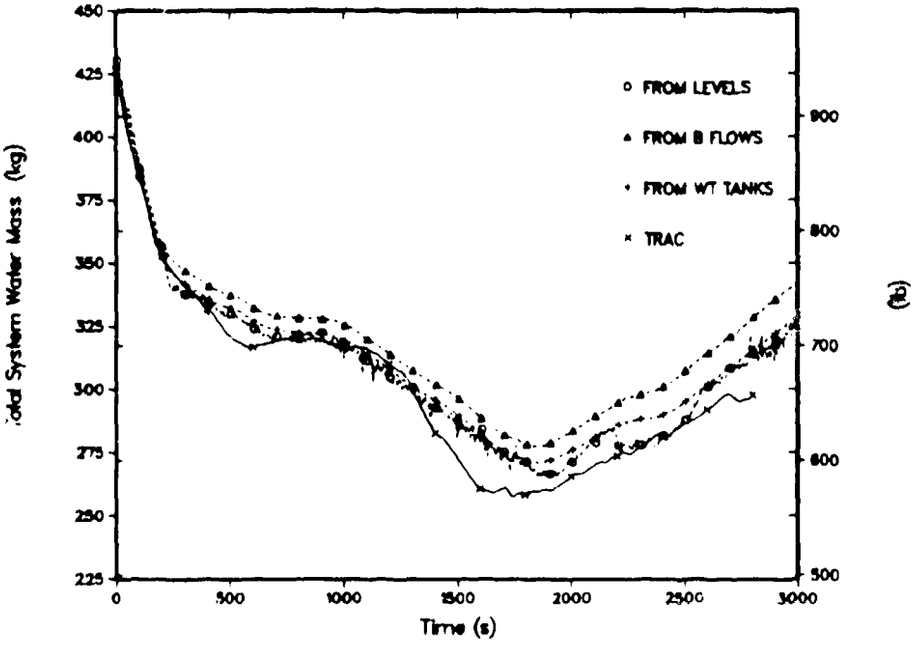

Fig. 25.
Test 320201 broken loop SG collapsed liquid levels

CFT was actuated on low pressure and fluid was discharged from the CFT into the upper downcomer. The calculation was terminated at 2800 s because at this time it was evident that the point of minimum primary system inventory had been surpassed.

Phase four began at 1760 s in the test and 1650 s in the calculation when the primary-system pressure (Fig. 19) decreased to the highest SG secondary pressure and the pressure control for both secondaries was switched into the 5.246×10^{-3} MPa/s (50 psi/min) blowdown mode. AFW flow was then restarted in both SGs to maintain the secondary level at the 9.63 m (31.6 ft) set point, and BCM heat transfer was reestablished since the SG primary levels (Figs. 24 and 25) were well below the AFW injection elevation. The primary depressurization rates were increased at these times in the test and the calculation (Fig. 19), causing the measured and calculated leak flows to fall below the HPI flows (Fig. 20). The calculated leak flow in Fig. 20 showed oscillations; the peaks of these oscillations corresponded to brief periods when the fluid at the leak site was subcooled. This difference between the measured and calculated leak flows probably resulted from differences in the CL flows. The integrated leak flow comparison was reasonable, however, as indicated by Fig. 21, which shows that the calculated refill rate during phase four compared well with the observed refill rate.

Figures 24 and 25 show that the measured and calculated SG secondary levels decreased from the 9.63 m (31.6 ft) set point at the beginning of phase four. The level decrease was caused by entrainment of the AFW liquid by the upward steam flow in the secondaries. The entrainment of the AFW while the secondaries were in the blowdown mode prevented the AFW from effectively controlling the secondary levels. This three-dimensional phenomenon was modeled with one-dimensional components in the calculation. Differences between the magnitude of the phenomenon the test and in the calculation are difficult to isolate because the steam flow measurements did not provide reliable data after the AFW was entrained into the steam lines (Ref. 3).

As the secondary pressures continued to decrease during phase four in the test, the SG blowdown depressurization was limited by the relief capacity of the secondary pressure control valves. Figure 19 shows that when the secondary pressures decreased below approximately 2.758 MPa (400 psi), the 5.246×10^{-3} MPa/s (50 psi/min) depressurization rate was no longer achieved. This behavior was modeled in the calculation by using the measured SG depressurization rate for the ATOG set point when the secondary pressure was below 2.758 MPa (400 psi). Figure 19 shows that the primary pressure followed the decreasing secondary pressures during phase four in both the test and the calculation.

Figure 26 shows that the CFT was actuated at 1865 s in the test and at 1755 s in the calculation when the primary system pressure decreased to 4.48 MPa (650 psia). The injection of liquid from the CFT into the upper downcomer enhanced the refilling of the primary (Fig. 21) which was already in progress at these respective times in the test and the calculation. The measured and calculated CFT levels were approximately the same since the primary depressurization rates were nearly the same below 4.48 MPa (650 psi).

The differences between Test 320201 and the posttest calculation discussed above were very similar to the differences noted for Test 3109AA. Again, there was evidence that the BCM heat transfer was too low in the calculation. This difference occurred during phase three in the intact-loop SG. Differences between the measured and calculated leak flows occurred over most of the 3000-s calculational period. These differences could be caused by deficiencies in the TRAC-PF1/MOD1 critical flow model, or by differences in the measured and calculated leak upstream conditions. To further isolate the cause of the leak flow differences would require measured data for the leak upstream pressure and the broken loop CL flow rates. The primary-system mass inventory comparison, however, indicates that the integrated leak flow was calculated correctly when the primary pressure was calculated correctly. Finally, the results for Test 320201 also indicate that the secondary heat or steam losses were too low in the TRAC-PF1/MOD1 input model. This shortened the duration of phase three in the calculation. Despite these differences, the overall comparison of the measured and calculated parameters for Test 320201 was reasonable.

CONCLUSIONS

The comparison of measured and calculated parameters for MIST Tests 3109AA and 320201 has shown that the physical phenomena which governed the course of these transients were also predicted in the calculations. The overall agreement between the tests and the calculations was reasonable: the major trends of the data were predicted correctly, although TRAC values were frequently outside the range of data uncertainty because of minor code/model deficiencies. With reasonable agreement, valid conclusions should still be reached if the code is used in similar applications.

Specific differences between measured and calculated parameters can be attributed to one of three categories of factors that can affect the calculated results. First, uncertainty in the data necessary to fully describe the facility and test operation can lead to uncertainty in the calculated results. Second, approximations in the code input model such as the resolution of the nodalization, time-step size, or the selection of a one-dimensional component vs a

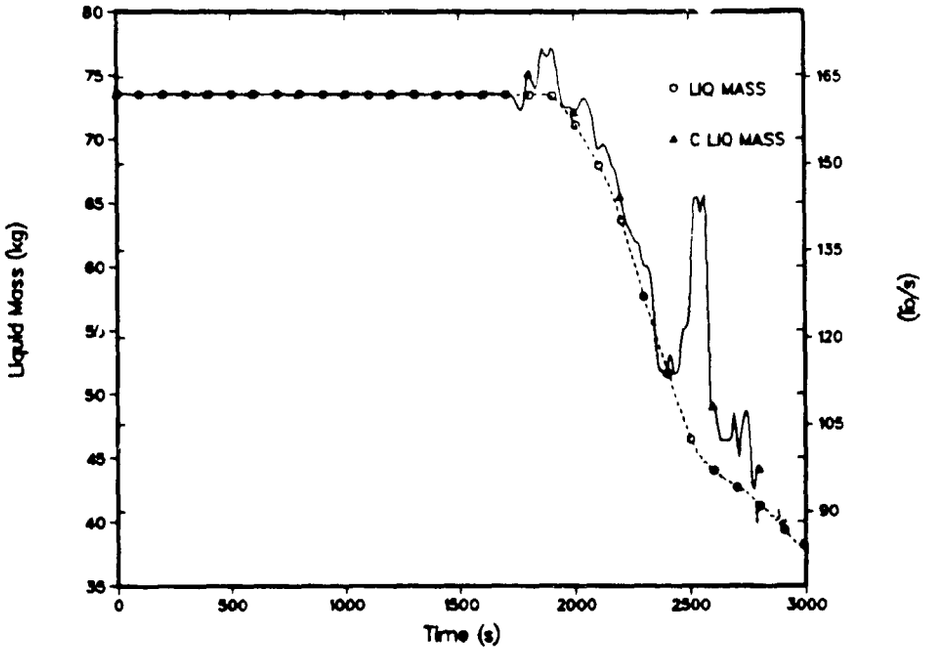

Fig. 26.
CFT mass.

three-dimensional component can affect calculated parameters. Third, the validity of the correlations and models in the code may affect the code calculations. Before conclusions can be drawn from code/data comparisons about the third category, code correlations and models, factors in the first two categories must be ruled out as possible causes for the differences between measured and calculated parameters.

Differences between MIST Tests 3109AA and 320201 were caused by factors from each category. Uncertainty in the secondary heat and steam losses in the MIST facility led to the inaccurate modeling of these losses. The losses were estimated to be 1.5 kW per steam line, which was not sufficient energy loss. This caused the secondary pressures in both calculations to increase when the measured remained constant. As a result, the duration of phase three was too short in each calculation and the phase four phenomena were shifted forward in time. Since both the 10-cm^2 calculation and the 50-cm^2 calculation were affected, it can be concluded that steam line heat-loss modeling is important for a wide range of SBLOCA leak sizes in the MIST facility. In general, if BCM is calculated to occur at the wrong time, the magnitude of the calculated BCM can be affected since the calculated SG primary levels generally vary with time. This, however, does not appear to be the case for the Test 3109AA and 320201 calculations.

The calculated results for both experiments were found to be very sensitive to the representation of the boundary conditions in the TRAC-PF1/MOD1 input model. In order to calculate the BCM phenomena as closely as possible, it was necessary to input the measured AFW flow for a period of several hundred seconds after SG refill. In the calculation for Test 3109AA, it was found that a subcooled leak flow multiplier of 0.87 was needed to accurately calculate the subcooled leak flow and phenomena that occurred before BCM.

Correlations and models in the code that cause differences between the test and calculation are often difficult to identify among the many factors that can affect the calculated parameters. The results of the Test 3109AA calculation, however, indicated that the TRAC-PF1/MOD1 critical flow model does not properly account for changes in upstream subcooling. Conclusions about the critical flow model cannot be drawn from Test 320201 because, with the higher leak flow, uncertainty in the frictional pressure losses upstream of the leak creates uncertainty in the leak upstream pressure during the test. Finally, the results indicated that the calculated BCM heat transfer was too low for both experiments. This could be caused by a heat-transfer correlation error, SG nodalization that was too coarse, or by an incorrectly determined flow regime during the calculation.

The code/data analyses presented herein constitute part of an assessment matrix for the performance of the TRAC-PF1/MOD1 code, which will ultimately be used to extrapolate data from the MIST facility to full-scale plant behavior.

REFERENCES

1. Safety Code Development Group, "TRAC-PF1/MOD1: An Advanced Best-Estimate Computer Program for Pressurized Water Reactor Thermal-Hydraulic Analysis," Los Alamos National Laboratory report LA-10157-MS, NUREG/CR-3858 (July 1986).
2. "MIST Test Specifications," Babcock & Wilcox document BAW-1894 (October 1985).
3. J. R. Gloudemans, *et al.*, "Group Report, MIST Test Group 32, Leak-HPI Configuration," Babcock and Wilcox document BAW-1964 (June 1987).